Molecular Crystals and Liquid Crystals

ISSN: 1542-1406 (Print) 1563-5287 (Online) Journal homepage: http://www.tandfonline.com/loi/gmcl20

Thermal Conductivity of Diglycidylester-Terminated Liquid Crystalline Epoxy/Alumina Composite

Thanhkieu Giang & Jinhwan Kim

To cite this article: Thanhkieu Giang & Jinhwan Kim (2016) Thermal Conductivity of Diglycidylester-Terminated Liquid Crystalline Epoxy/Alumina Composite, Molecular Crystals and Liquid Crystals, 629:1, 12-26, DOI: 10.1080/15421406.2015.1107816

To link to this article: http://dx.doi.org/10.1080/15421406.2015.1107816

Published online: 16 Jun 2016.

MOLECULAR CRYSTALS AND LIQUID CRYSTALS
2016, VOL. 629, 12–26
http://dx.doi.org/10.1080/15421406.2015.1107816

Taylor & Francis
Taylor & Francis Group

Thermal conductivity of diglycidylester-terminated liquid crystalline epoxy/alumina composite

Thanhkieu Giang and Jinhwan Kim

Department of Polymer Science and Engineering, Sungkyunkwan University, Suwon, Gyeonggi-do, Republic of Korea

ABSTRACT

We synthesized three novel diglycidylester-terminated liquid crystalline epoxy (LCE) resins containing various liquid crystalline backbones to investigate the thermal conductivity of composites filled with alumina (Al_2O_3) particles and the results are compared to that of the composite with diglycidylether-terminated LCE resin which differs only in the structure of terminal epoxy linkage. The results showed that LCE resins displayed distinct nematic liquid crystalline phases at wide temperature ranges and all cured systems exhibited well-reserved nematic phases. The thermal conductivity of novel diglycidylester-terminated LCE resin containing composite is higher than that of diglycidylether-terminated LCE resin containing composite.

KEYWORDS

Alumina; composite; liquid crystalline epoxy; mesophase; thermal conductivity

Introduction

Epoxy resins are the most widely used polymeric materials for electronic packaging applications because they are relatively cheap and their processing ability is excellent. The use of epoxy resins, however, is restricted in some specific electric and electronic parts that require high thermal dissipation due to their low thermal conductivity. Thus the high thermal conductive filler, typically Al_2O_3 is incorporated into epoxy matrix, making epoxy/Al_2O_3 composites. Most commonly used epoxies for this approach are bisphenol A epoxy [1–4], phenol novolac epoxy [5], cycloaliphatic epoxy [6, 7], and siloxane epoxy [8, 9]. The thermal conductivities of composites based on these epoxies, nevertheless, are not sufficient to satisfy the heat dissipation requirements of electric devices such as high power LED, which grows very rapidly in nowadays industrial markets.

This thermal dissipation problem can be solved very effectively by improving the thermal conductivity of epoxy resin itself [10]. It was reported that the use of LCE having a highly ordered structure could be a practical solution to achieve this purpose. LCE resin that contains mesogenic groups in its backbone can form a self-ordered structure during curing process. The highly ordered network structure of the LCE resin enhances the thermal conductivity of the composite due to more effective thermal energy transmission in the ordered structure.

CONTACT Jinhwan Kim jhkim@skku.edu
Color versions of one or more of the figures in the article can be found online at www.tandfonline.com/gmcl.

Table 1. Characteristics of LCE resins employed in this study.

Structure	Name	Yield (%)	EEW (g/eq)	T_m (°C)
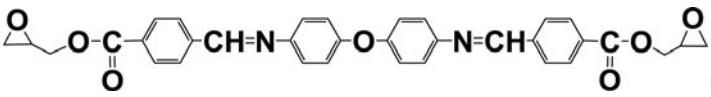	LCE-DPEs	80	348	202
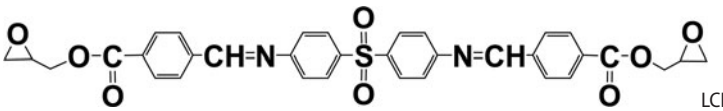	LCE-DPSs	59	344	191
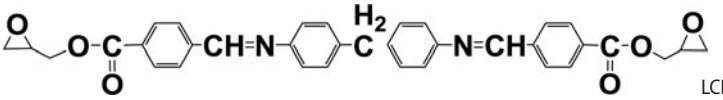	LCE-DPMs	77	373	158
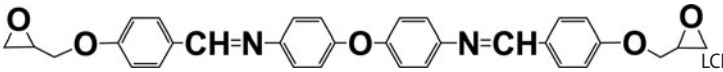	LCE-DPE	71	350	240

During the past two decades, numerous studies have been carried out to investigate the synthesis, curing behavior, and mechanical properties of LCE resins containing various mesogenic units in backbone structure, such as azine [11], azo [12, 13], azomethine [14–18], binaphthyl [19, 20], biphenyl [21–24], ester [25–30], and stilbene [31–38]. However, most of studies have focused on diglycidylether-terminated LCE resins. Only a few studies have been reported on the synthesis and thermal property of LCE terminated with diglycidylester.

In this study, we synthesized three novel diglycidylester-terminated LCE resins (designated as LCE-DPEs, LCE-DPSs, and LCE-DPMs, where the last letter "s" represents "ester") to investigate the thermal conductivities of LCE/ Al_2O_3 composites. The chemical structures and characteristics of materials employed in this study are given in Table 1. For comparison reason, one diglycidylether-terminated LCE resin (designated as LCE-DPE) was also employed. 4,4′-diaminodiphenyl sulfone (DDS) was used as a curing agent and 2-methylimidazole (2MI) was added as a catalyst. $Al_2O_3$of a commercial source was applied as an inorganic filler. The thermal conductivities of cured composites were experimentally determined and compared with values predicted by Agari-Uno's theoretical model [39, 40].

Experimental

Materials

Epichlorohydrin, tetrabutylammonium bromide (TBAB), 4-carboxybenzaldehyde, 4-hydroxybenzaldehyde, 4,4'-oxydianiline, 4,4'-diaminodiphenyl methane, and DDS were purchased from Aldrich. N,N-dimethylacetamide, methanol, ether, and other basic chemicals were purchased from Samchun Chemical Company, Korea. 2MI and a commercial grade Al_2O_3 with a mean diameter of 5μm were provided by LG Innotek, Korea. The Al_2O_3 had a spherical shape. All chemicals were used without further purification.

Synthesis of liquid crystalline epoxies

Three novel LCE species (LCE-DPEs, LCE-DPSs, and LCE-DPMs) containing various backbones were synthesized. The synthetic schemes are presented in Scheme 1. The yield, epoxy equivalent weight (EEW), and melting temperature (T_m) are given in Table 1. The success of

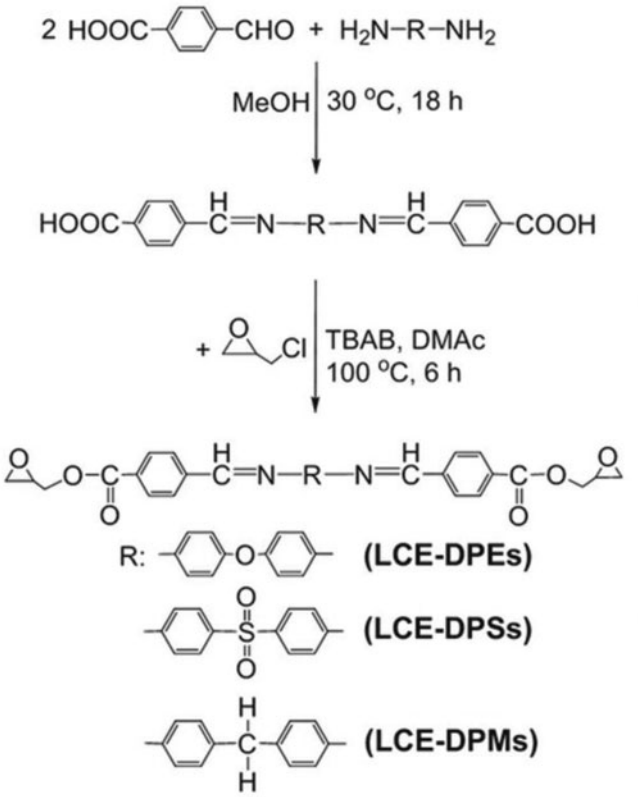

Scheme 1. Synthetic scheme for LCE resins employed in this study.

synthesis was confirmed by ^{1}H-NMR and FT-IR, which results are given in Figs. 1–3. LCE-DPE was synthesized according to the procedure reported in our previous work [41].

Synthesis of intermediate product: 4′4′-bis(4-carboxybenzylidene)-diaminodiphenyl ether (DPEs), 4′4′-bis(4-carboxybenzylidene)-diaminodiphenylsulfone (DPSs), and 4′4′-bis(4-carboxybenzylidene)-diaminodiphenylmethane (DPMs)

4-carboxybenzaldehyde (0.2 mol) was dissolved in methanol and placed to a 250 ml three-neck round-bottom flask at 30°C. Diamine (0.1 mol) dissolved in methanol was added dropwise with vigorous stirring at 30°C. The solution was stirred at that temperature for 18 h. The precipitated yellow solid was filtered and sequentially washed several times with methanol and ether. The product was dried at 50°C in a vacuum. The yield was 94% for DPEs, 96% for DPSs, and 96% for DPMs.

Synthesis of 4′4′-bis(4-carboxybenzylidene)-diaminodiphenylether diglycidylester (LCE-DPEs), 4′4′-bis(4-carboxybenzylidene)-diaminodiphenylsulfone diglycidylester (LCE-DPSs), and 4′4′-bis(4-carboxybenzylidene)-diaminodiphenylmethane diglycidylester (LCE-DPMs)

A mixture of intermediate product (0.02 mol), DMAc (50 ml), and epichlorohydrin (1.00 mol) was placed into a 250 ml three-necked round-bottom flask that was equipped with a temperature controller, a reflux condenser, a heating oil bath, and a mechanical stirrer at room temperature. The mixture was slowly heated to 100°C and TBAB was added as a catalyst.

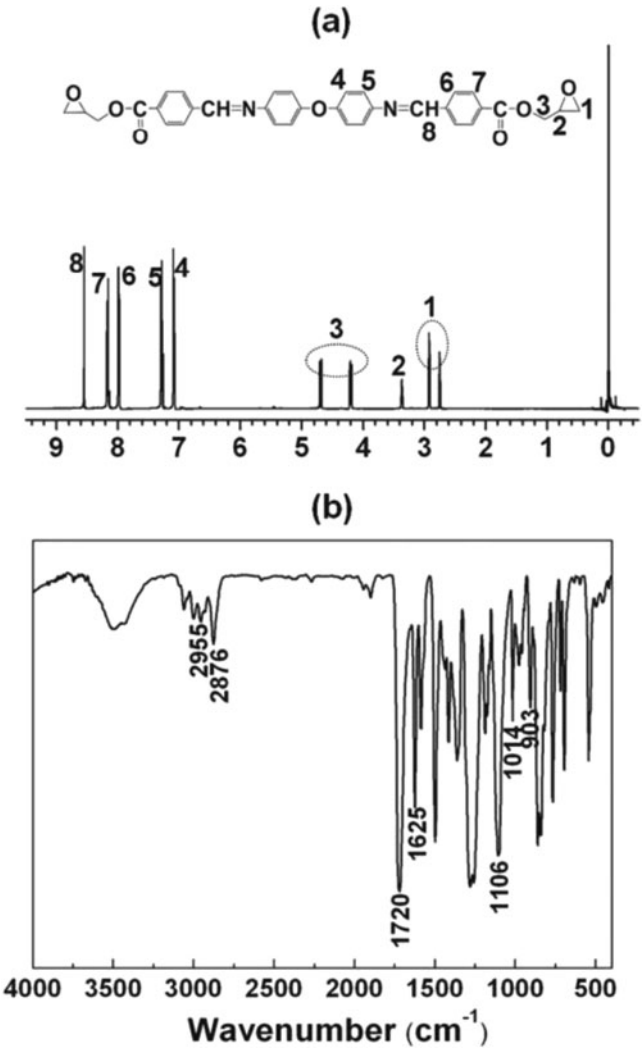

Figure 1. ^{1}H-NMR (a) and FT-IR (b) spectra of synthesized LCE-DPEs.

The solution was stirred at that temperature for 6 h. After cooling to room temperature, the reaction mixture was poured into methanol. A yellow solid was collected and continuously washed with deionized water and methanol. The product was dried at 40° C in a vacuum.

[LCE-DPEs] ^{1}H-NMR ($CDCl_3$ -d_6, ppm): δ = 8.55 (s, 2H), δ = 8.16–8.17 (d, 4H), δ = 7.98–7.99 (d, 4H), δ = 7.28–7.30 (d, 4H), δ = 7.08–7.09 (d, 4H), δ = 4.68–4.71 (d, 2H), δ = 4.18–4.26 (m, 2H), δ = 3.35–3.39 (m, 2H), δ = 2.91–2.93 (m, 2H), and δ = 2.74–2.76 (m, 2H). FT-IR: 2955, 2876 cm −1 (CH_2); 1720 cm^{-1} (C=O); 1625 cm^{-1} (C=N); 1106 cm^{-1} (C–O); 1014 cm^{-1} (ether); 903 cm^{-1} (epoxy ring).

[LCE-DPSs] ^{1}H-NMR ($CDCl_3$ -d_6, ppm): δ = 8.44 (s, 2H), δ = 8.16–8.19 (d, 4H), δ = 7.95–7.98 (d, 4H), δ = 7.98–8.00 (d, 4H), δ = 7.26–7.28 (d, 4H), δ = 4.67–4.72 (d, 2H), δ = 4.17–4.25 (m, 2H), δ = 3.33–3.38 (m, 2H), δ = 2.90–2.93 (m, 2H), and δ = 2.73–2.75 (m, 2H). FT-IR: 2955, 2889 cm^{-1} (CH2); 1717 cm^{-1} (C=O); 1629 cm^{-1} (C=N); 1106 cm^{-1} (C–O); 1014 cm^{-1} (ether); 891 cm^{-1} (epoxy ring).

[LCE-DPMs] ^{1}H-NMR ($CDCl_3$ -d_6, ppm): δ = 8.53 (s, 2H), δ = 8.14–8.17 (d, 4H), δ = 7.96–7.98 (d, 4H), δ = 7.24–7.26 (d, 4H), δ = 7.19–7.21 (d, 4H), δ = 4.67–4.70 (d, 2H), δ

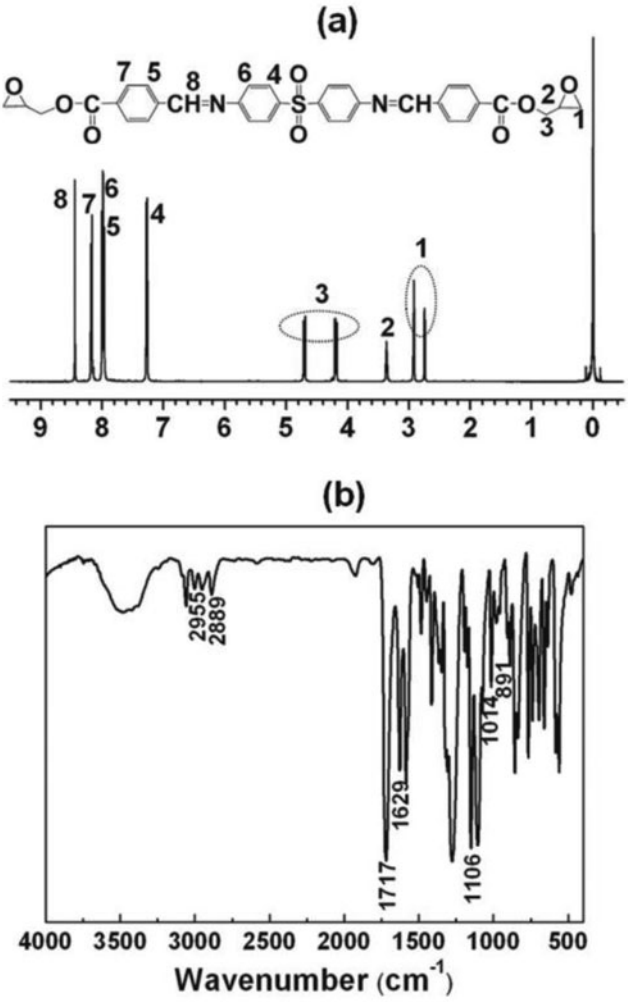

Figure 2. [1]H-NMR (a) and FT-IR (b) spectra of synthesized LCE-DPSs.

= 4.18–4.22 (m, 2H), δ = 3.35–3.38 (m, 2H), δ = 2.90–2.92 (m, 2H), and δ = 2.73–2.75 (m, 2H). FT-IR: 2949, 2879 cm^{-1} (CH_2); 1717 cm^{-1} (C=O); 1619 cm^{-1} (C=N); 1109 cm^{-1} (C–O); 1014 cm^{-1} (ether); 903 cm^{-1} (epoxy ring).

Measurements and sample preparation

Spectroscopic analysis

[1]H-NMR analysis was performed on a Varian Unity Inova 500NB spectrometer using $CDCl_3$ -d_6 as a solvent and tetramethylsilane (TMS) as a reference. The infrared (IR) spectra were obtained using a Nicolet 380 FT-IR spectrometer with KBR pellets.

Thermal analysis

Thermogravimetric analysis (TGA) was performed on 2 to 10 mg samples under a nitrogen atmosphere at a heating rate of 10°C/min using a TA instruments 2050 thermogravimetric analyzer. Differential scanning calorimetry (DSC) was performed on 3 to 5 mg samples under

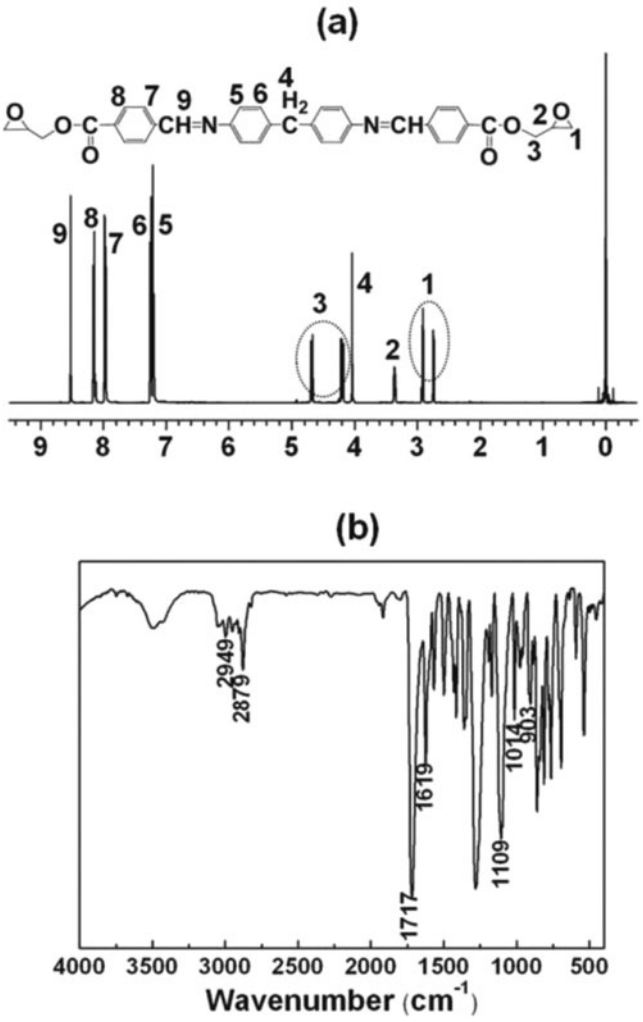

Figure 3. ^{1}H-NMR (a) and FT-IR (b) spectra of synthesized LCE-DPMs.

a nitrogen atmosphere at a heating rate of 10°C/min using a TA instruments 2910 DSC analyzer.

Morphology Observation

Morphological features of the starting component and cured composite were observed using an Optical microscope (OM) equipped with crossed polarizers in transmitted light mode.

Wide-angle X-ray diffraction

Wide-angle X-ray diffraction (WAXD, D8 discover) using Cu(Kα) radiation was used to determine liquid crystalline characteristics and d-spacing of cured LCE/DDS mixture. The tube source was operated at 1.6 kW with scanning speed of 5°/min and sample interval of 0.05°.

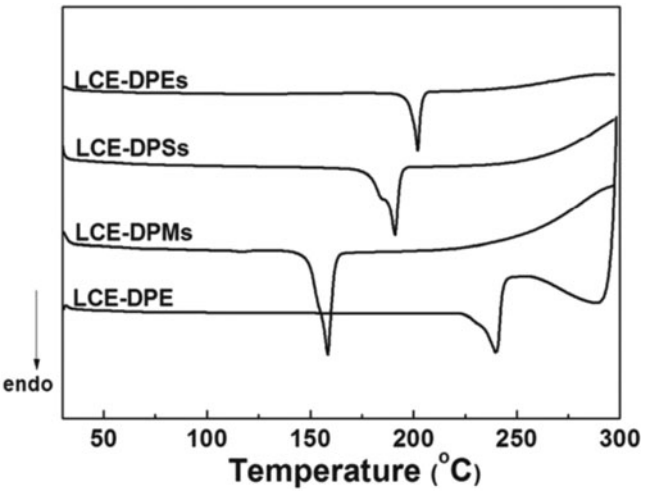

Figure 4. DSC thermograms of synthesized LCE resins.

Sample preparation for thermal conductivity measurement

A mixture of epoxy, curing agent, and catalyst at the designated composition was dissolved in N,N-dimethylacetamide. The mixture was shaken using a paste mixer machine. Then a designated amount of Al_2O_3 was added and the resulting mixture was shaken again. The solvent was removed by placing the sample in a vacuum oven at a pre-determined temperature for 24 h. Samples were molded by a hot press at a pressure of 2500 psi. The LCE-DPEs/DDS system was cured at 210°C for 30 minutes. The LCE-DPSs/DDS system was cured at 180°C for 30 minutes. The LCE-DPMs/DDS and LCE-DPs/DDS systems were cured at 170°C for 30 minutes. The specimen had a diameter of 12.7 mm and thickness of 1.0 mm.

Thermal conductivity measurement

The thermal conductivity (λ) was determined from the formula:

$$\lambda = \alpha \times \delta \times \mathbf{C}_p,$$

where α, δ, and C_p represent the thermal diffusivity, density, and heat capacity of the test specimen at 25°C, respectively. The thermal diffusivity was measured using laser flash method employing a LFA 447 flash diffusivity instrument (NETZSCH-Gerätebau GmbH). C_p was determined separately by DSC at a temperature range of 0 to 100°C at a heating rate of 10°C/min.

Results and discussion

Characteristics of synthesized LCE resins

The thermal behaviors and mesomorphic properties of synthesized LCE resins differing in mesogenic backbone moieties were examined using DSC, TGA, and OM. DSC thermograms of the LCE resins recorded under dynamic conditions are presented in Fig. 4. It is observed that LCE-DPE has very broad endothermic peak at 240°C, which corresponds to the melting (T_m) of liquid crystalline structure of this compound (melting enthalpy (ΔH_m) = 42.8 kJ

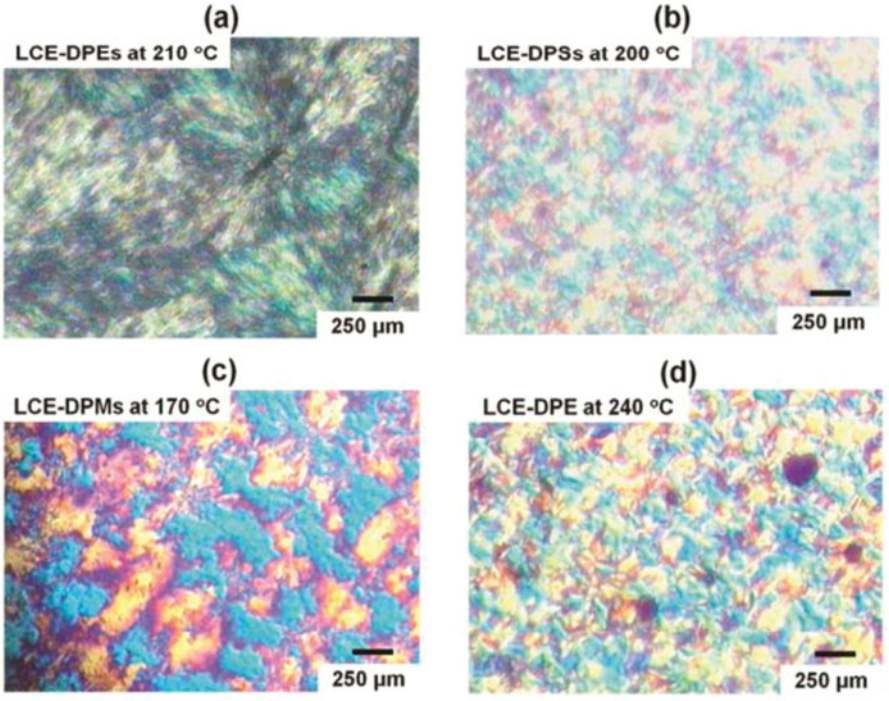

Figure 5. Morphologies of LCE resins observed by optical microscopes.

mol^{-1} and melting entropy (ΔS_m) = 83.4 J mol^{-1} K^{-1}). However, LCE-DPE does not show any other endotherm transition above T_m related to the change into isotropic phase. Instead, very distinct exotherm responsible for the homopolymer reaction and crosslinking of this LCE resin at nematic phase is observed. Thus, it is concluded that the temperature range at which LCE-DPE remains mesophase is quite narrow and the nematic phase presented in Fig. 5d, which is observed by OM, becomes isotropic phase in a very short time of heating above 240°C. On the other hand, LCE-DPEs, LCE-DPSs, and LCE-DPMs show distinct endothermic peaks that correspond to the melting of liquid crystalline structures. LCE-DPEs shows the highest T_m at 202°C (ΔH_m = 66.3 kJ mol^{-1} and ΔS_m = 139.6 J mol^{-1} K^{-1}). The T_m of LCE-DPSs is observed at 191°C (ΔH_m = 45.4 kJ mol^{-1} and ΔS_m = 97.8 J mol^{-1} K^{-1}) and the T_m of LCE-DPMs at 158°C (ΔH_m = 57.2 kJ mol^{-1} and ΔS_m = 132.7 J mol^{-1} K^{-1}). The nematic mesophases are clearly observed above T_m for these LCE resins by optical microscopy analysis and the results are shown in Fig. 5a–c. However, this liquid crystalline mesophases change into isotropic phases above the temperature given in Fig. 5, meaning that the mesophase ranges of these LCE resins are quite narrow. It is worth noting that the DSC thermograms of ester-terminated LCE resins also show an exothermic reactions beginning at about 250°C which can be assignable to the homopolymerization of these LCE resins. The homopolymerization of epoxy containing azomethine group was reported to be proceeded by anionic polymerization mechanism [42, 43]. Interestingly enough, the beginning temperature at which the homopolymerization takes place increases in the following order: LCE-DPMs > LCE-DPSs > LCE-DPEs > LCE-DPE. Exactly the same sequence is observed for the T_m of these LCE resins. From these results, it is concluded that the mesophase range is much broader and the nematic mesophase is more stable for diglycidylester-terminated

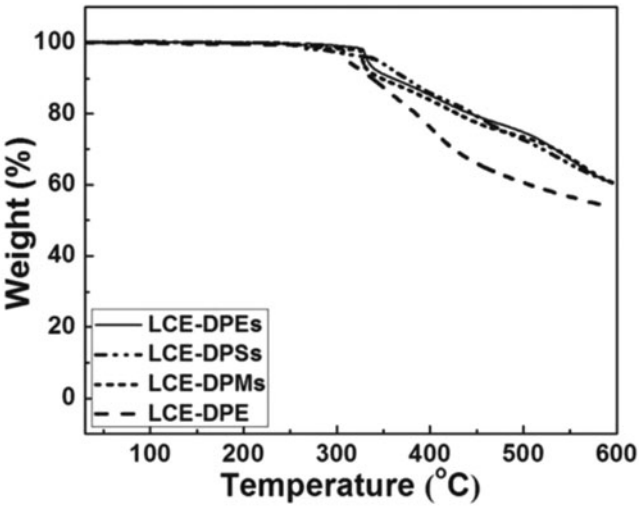

Figure 6. TGA thermograms of synthesized LCE resins.

LCE compared to diglycidylether-terminated LCE. Subsequently, the thermal degradation behaviors of LCE resins were investigated and the results are shown in Fig. 6. All LCE resins thermally decompose in one step with an onset degradation temperature of around 300°C. Diglycidylester-terminated LCE resins leave slightly higher proportion of residual chars than diglycidylether-terminated LCE resin. These findings also confirm that the ester-terminated compounds are more thermally stable in the mesophase range compared to ether-terminated compound.

Now, main difference in the thermal transition of the liquid crystalline structures between ester- and ether-terminated LCEs and the effect of backbone moiety in ester-terminated LCE resins will be discussed. Comparing the T_m of LCE-DPEs and LCE-DPE in Fig. 4, it is concluded that the T_m of ester-terminated compound is lower than that of ether-terminated compound. Since LCE-DPEs and LCE-DPE have the same liquid crystalline moiety in backbone structure but differ only in their structural units connecting to epoxide ring. The above mentioned difference is believed to be resulted from the increased flexibility of ester-terminated LCE compared to ether-terminated LCE. It is quite interesting to compare the T_m of three ester-terminated LCEs (LCE-DPEs, LCE-DPSs, and LCE-DPMs) differing in backbone moiety of liquid crystalline structures. The results shown in Fig. 4 clearly indicate that the flexibility of backbone moiety is the most important factor governing the thermal transition behaviors of LCE resins.

Curing behaviors of LCE resins with DDS

The curing behaviors of different LCE resins with an identical curing agent, DDS were investigated using DSC. For the experiments, DDS at the equimolar ratio was employed and the same amount (3 mol% to epoxy) of 2MI was added as an accelerator. Figure 7 shows the dynamic curing processes of different LCE/DDS mixtures. Very broad exotherm with T_{onset} of 197°C and T_{peak} of 218°C, which are originated from the curing reaction of LCE-DPEs and DDS, is observed in the dynamic thermogram of the LCE-DPEs/DDS mixture and no clear endotherm is observed. Remembering that the T_m of LCE-DPEs is

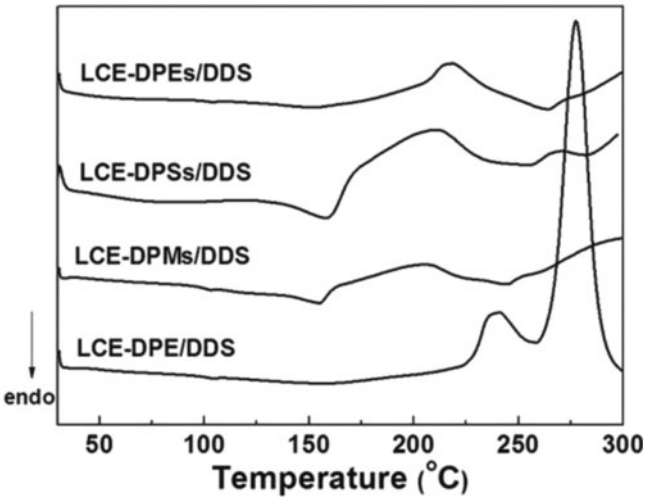

Figure 7. Dynamic DSC thermograms of different LCE/DDS systems.

202°C, this observation indicates that the curing of LCE-DPEs and DDS occurs prior to the melting of LCE-DPEs. An endothermic peak at 158°C is observed for the LCE-DPSs/DDS mixture, implying that the curing reaction starts in the solid state of this compound. The exotherm at 207°C is assigned to the cure of LCE-DPSs/DDS mixture. The DSC curve of the LCE-DPMs/DDS mixture shows a melting peak at 154°C, which corresponds to the melting of LCE-DPMs itself. Broad exotherm with T_{peak} around 205°C is attributed to the curing reaction between LCE-DPMs and DDS. The three systems show additional exothermic reaction above 250°C, which is believed to be related to the homopolymerization among epoxies.

The curing reaction between the oxirane ring of epoxy and amine is proceeded by a nucleophilic substitution reaction. The epoxy ring reacts with the primary amine to produce the secondary amine in the initial curing stage, then the other epoxy group further reacts with the secondary amine and subsequently crosslinking is carried out between the epoxy and hydroxyl groups generated from reaction. In this study, the same curing mechanism should prevail for all mixtures since an identical curing agent was used for all systems. On the other hand, it should be noted that there are differences in the backbone moieties of three ester-terminated LCE resins. A diphenylether group is present in both LCE-DPE and LCE-DPEs while LCE-DPSs and LCE-DPMs possess diphenylsulfone and diphenylmethane group, respectively. The sulfone unit in LCE-DPSs has a greater electron-withdrawing tendency in comparison to the methylene unit in LCE-DPMs and the ether unit in LCE-DPEs. The difference in electron-withdrawing power will affect the electron density of the oxirane ring and consequently leads to different chemical reactivity in the following order: LCE-DPSs > LCE-DPMs > LCE-DPEs. Thus, the heat of curing of LCE-DPSs/DDS is the highest and that of LCE-DPEs/DDS is the lowest among the three systems. The heats of curing for four LCE/DDS systems measured by dynamic DSC experiments are summarized in Table 2. The heat of curing is the lowest for LCE-DPE/DDS among four LCE/DDS systems investigated in this study. From Figs. 4 and 7, not only T_m of LCE-DPE itself but also T peak of LCE-DPE/DDS mixture are observed around 240°C. Considering that the homopolymerization of LCE-DPE begins at 250°C, the results shown in Fig. 7 indicate that the curing reaction resulted from the reaction

Table 2. Thermal properties related to the curing of LCE resins with DDS.

System	T_{onset} (°C)	T_{peak} (°C)	Heat of curing (J/g)
LCE-DPEs/DDS	197	218	101
LCE-DPSs/DDS	176	207	131
LCE-DPMs/DDS	167	205	124
LCE-DPE/DDS	228	238	37

between LCE-DPE and DDS is relatively minor and the major curing reaction comes from the homopolymerization of LCE-DPE.

Morphologies of cured LCE/DDS mixtures

To observe the morphologies of the cured specimens, the optical microscopy was employed and the results are given in Fig. 8. The stoichiometric mixture of LCE and DDS with the same amount of accelerator (3 mol% to epoxy) was cured by following the curing schedules presented in Fig. 8. The curing schedules were chosen by analyzing the curing behaviors shown in Fig. 7 and also employed to prepare the specimens for the thermal conductivity measurements whose results are presented in Fig. 10. The optical microscopic images under cross polarized light were taken from the specimens without filler for the sake of clear observation. As can be seen in Fig. 8d, birefringence regions and black isotropic phase are observed for the cured LCE-DPE/DDS system, indicating that it is consisted of two phases: crystalline solid phase of LCE-DPE whose T_m is 240°C and isotropic mixture of LCE-DPE

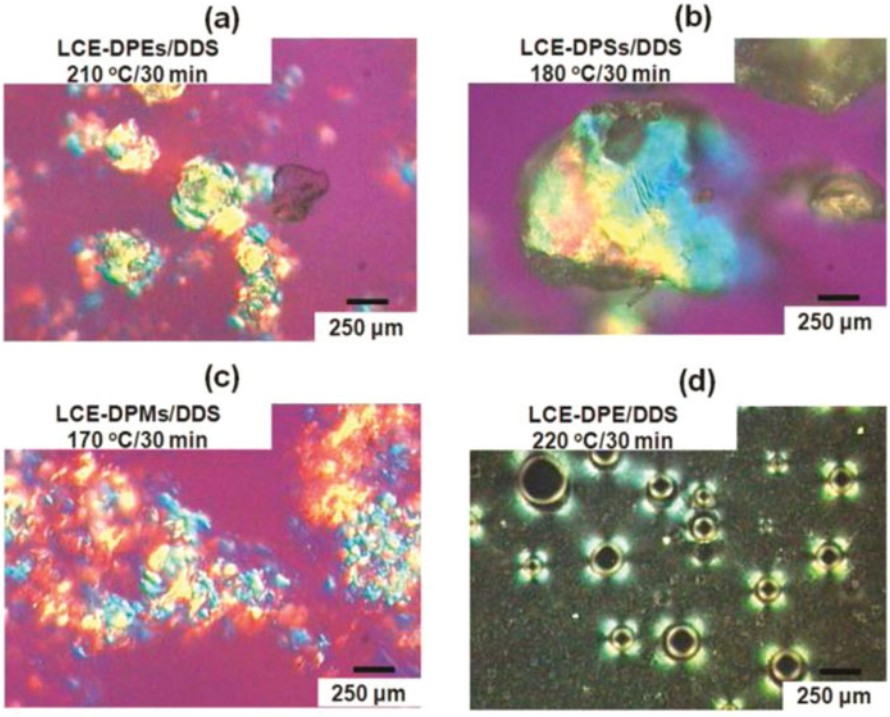

Figure 8. Optical micrographs of cured LCE/DDS systems.

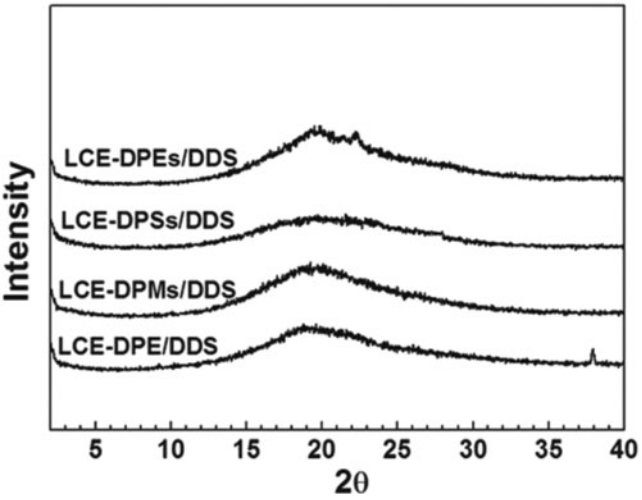

Figure 9. WAXD patterns of cured LCE/DDS systems.

and DDS (T_m of DDS is 176°C when measured by DSC). On the other hand, in Fig. 8a–c, the nematic mesophases are clearly observed for LCE-DPEs/DDS, LCE-DPSs/DDS, and LCE-DPMs/DDS mixtures when cured just above the T_m of corresponding LCE resin. These results indicate that the mesophasic liquid crystalline structures are well reserved for the cured specimens of three ester-terminated LCEs when cured with DDS at the designed curing schedules.

To investigate more the domain structure of cured LCE/DDS mixtures, the wide-angle X-ray diffraction pattern was measured for the identical cured specimens and the results are illustrated in Fig. 9. For all cured systems, very broad peaks around 19.9° are observed over a wide angle of 2θ.

The plane space calculated from $2\theta = 19.9°$ is 4.5 Å, which is characteristic of a nematic mesophase. On the other hand, no peaks derived from the smectic liquid crystalline phase are observed at a low 2θ angle. These findings demonstrate that all cured systems consist of polydomain structures and each domain retains a nematic mesophase.

Thermal conductivity of LCE/DDS/Al_2O_3 composite

The thermal conductivities of various LCE/DDS/Al_2O_3 composites as a function of alumina amount were experimentally determined and the results are presented in Fig. 10. The results clearly show that the thermal conductivity of composite linearly increase with filler loading as expected. At the same filler loading, the thermal conductivity of the composite is the lowest for the LCE-DPE/DDS system and no big difference is observed for the LCE-DPEs/DDS, LCE-DPSs/DDS, and LCE-DPMs/DDS systems. The thermal conductivity of the LCE-DPE/DDS/Al_2O_3 composite is determined to be 2.83 W/mK with an Al_2O_3 loading of 50 vol%, which is 9.1% lower than that of the LCE-DPEs/DDS/ Al_2O_3 composite at the same filler loading. From these results, it is concluded that the thermal conductivity of diglycidylester-terminated LCE containing composite, which exhibits mesophase at wider temperature ranges, is higher than that of diglycidylether-terminated LCE containing composite. It implies that the highly ordered structure of LCE has a positive effect on suppressing phonon scattering which plays an important role in the heat conduction and consequently enhances the thermal conductivity of the composite.

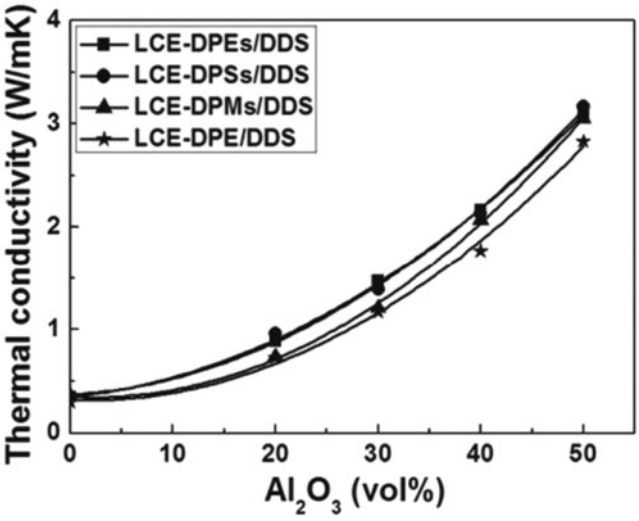

Figure 10. Thermal conductivities of various LCE/DDS/ Al_2O_3 composites as a function of filler content.

To evaluate the intrinsic thermal conductivity of neat LCE, the Agari-Uno model is employed for the theoretical prediction. Our previous study manifestly revealed that very good agreements between experimental data and the values calculated by the theoretical model are obtained for various epoxy/ Al_2O_3 composites. In this work, the thermal conductive values were measured experimentally using the laser flash method and compared with the values predicted by the Agari-Uno model and the results are presented in Fig. 11. The model provides a fairly good fit with experimental data for all systems. As a conclusion, the thermal conductivity of 0.35 W/mK is obtained for the neat LCE-DPEs and 0.39 W/mK for the neat LCE-DPSs and LCE-DPMs. It should be mentioned that the value of 0.19 W/mK was reported for the intrinsic thermal conductivity of most commonly used epoxy, diglycidylether of bisphenol A (DGEBA).

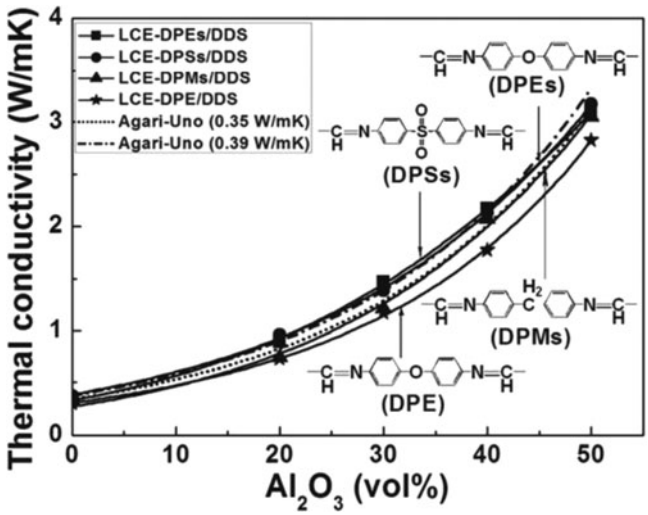

Figure 11. Thermal conductivity plots of LCE/DDS/ Al_2O_3 composites as a function of filler content: (symbols and full lines) experimental; (broken lines) calculated by adopting Agari-Uno model.

Conclusions

In this study, three novel diglycidylester-terminated LCE resins containing various liquid crystalline backbones were prepared to investigate the thermal conductivities of their composites with Al_2O_3 and the results are compared with the composite with diglycidylether-terminated LCE resin. At the same amount of Al_2O_3 loading, the thermal conductivity of composite increased in the order of LCE-DPEs ≈ LCE-DPSs > LCE-DPMs > LCE-DPE, indicating that the thermal conductivity of ester-terminated LCE containing composite is higher than that of ether-terminated LCE containing composite. The reason why the higher thermal conductivity is obtained for the ester-terminated LCE resin is not clear at this moment and more study is needed to elucidate this finding. The experimental data fitted quite well with the values calculated using the Agari-Uno model. 0.35 – 0.39 W/mK was obtained for the neat diglycidylester-terminated LCE resins, which is about twice higher than that (0.19 W/mK) of most commonly used epoxy, diglycidylether of bisphenol A (DGEBA). This result clearly demonstrated that the epoxy backbone structure is essential to achieve high thermal conductivity in the composite.

Acknowledgments

The authors appreciate the financial support from the LG Innotek, Korea.

References

[1] Zeng, J., Fu, R., Zhang, S., Song, X., & He, H. (2009). *J. Elec. Pack.*, *131*, 1.
[2] Shimazaki, Y., Hojo, F., & Takezawa, Y. (2009). *Appl. Mat. Inter.*, *1*, 225.
[3] Fu, J., Shi, L., Zhang, D., Zhong, Q., & Chen, Y. (2010). *Polym. Eng. Sci.*, *50*, 1809.
[4] Fua, J. F., Shi, L. Y., Zhong, Q. D., Chen, Y., and Chen, L. Y. (2011). *Polym. Adv. Technol.*, *22*, 1032.
[5] Kim, W., & Bae, J. (1999). *Polym. Eng. Sci.*, *39*, 756.
[6] Wong, C. P., & Bollampally, R. S. (1999). *J. Appl. Polym. Sci.*, *74*, 3396.
[7] Yu, J., et al. (2011). *Polym. Chem.*, *2*, 1380.
[8] Im, H., & Kim, J. (2011). *Carbon.*, *49*, 3503.
[9] Im, H., & Kim, J. (2011). *J. Mater. Sci.*, *46*, 6571.
[10] Giang, T., Park, J., Cho, I., Ko, Y., & Kim, J. (2013). *Polym. Comp.*, 34, 468.
[11] Yu, Y., et al. (2006). *J. Appl. Polym. Sci.*, *101*, 4366.
[12] Castell, P., Galià, M., & Serra, A. (2001). *Macromol. Chem. Phys.*, *202*, 1649.
[13] Koscielny, B., Pfitzmann, A., & Fedtke, M. (1994). *Polymer Bull.*, *32*, 529.
[14] Gao, Z., Yu, Y., Xu, Y., & Li, S. (2007). *J. Appl. Polym. Sci.*, *105*, 1861.
[15] Ochi, M., & Takashima, H. (2001). *Polymer*, *42*, 2379.
[16] Mija, A., Navard, P., Peiti, C., Babor, D., & Guigo, N. (2010). *Euro. Polym.*, *46*, 1380.
[17] Choi, E. J., Ahn, H., Lee, J. K., & Jin, J. (2000). *Polymer*, *41*, 7617.
[18] Ribera, D., Mantecón, A., & Serra, A. (2001). *Macromol. Chem. Phys.*, *202*, 1658.
[19] Mititelu-Mija, A., Cascaval, C. N., & Navard, P. (2005). *Design. Monom. Polym.*, *8*, 487.
[20] Yu, Y., et al. (2006). *J. Appl. Polym. Sci.*, *101*, 4366.
[21] Su, W. A. (1993). *J. Polym. Sci.: Part A. Polym. Chem.*, *31*, 3251.
[22] Lin, C., & Chien, L. (1995). *Macromol. Rapid Commun.*, *16*, 869.
[23] Mititelu, A., & Cascaval, C. N. (2005). *Polym. Plast. Tech. Eng.*, *44*, 151.
[24] Mallon, J. J., & Adams, P. M. (1993). *J. Polym. Sci.: Part A Polym. Chem.*, *31*, 2249.
[25] Zheng, Y., Ren, S., Ling, Y., & Lu, M. (2006). *Mol. Cryst. Liq. Cryst.*, *452*, 3.
[26] Lee, J. Y., & Jang, J. (2006). *Polymer*, *47*, 3036.
[27] Gao, J., Hou, G., Wang, Y., Li, H., & Liu, Y. (2006). *Polym. Plast. Tech. Eng.*, *45*, 947.
[28] Cai, Z., Sun, J., Zhou, Q., & Xu, J. (2007). *J. Polym. Sci.: Part A: Polym. Chem.*, *45*, 727.
[29] Cai, Z., Sun, J., Wang, D., & Zhou, Q. (2007). *J. Polym. Sci.: Part A: Polym. Chem.*, *45*, 3922.

[30] Pottie, L., Costa-Torroa, F., Tessier, M., Davidson, P., & Fradet, A. (2008). *Liquid Cryst*., *35*, 913.
[31] Ortiz, C., Kim, R., Rodighiero, E., Ober, C. K., & Kramer, E. J. (1998). *Macromolecules*., *31*, 4074.
[32] Ambrogi, V., Carfagna, C., Giamberini, M., Amendola, E., & Douglas, E. P. (2002). *J. Adhesion Sci. Technol.*, *16*, 15.
[33] Mihara, T., Nishimiya, Y., & Koide, N. (1998). *J. Appl. Polym. Sci*., 68, 1979. 16.
[34] Cho, S., Douglas, E. P., & Lee, J. Y. (2006). *J. Polym. Eng. Sci.*, 623.
[35] Bruggeman, A., Damman, S. B., & Tinnemans, A. H. A. (1997). *J. Appl. Polym. Sci.*, *66*, 1971.
[36] Sue, H. J., Earls, J. D., & Hefner, R. E. (1997). *J. Mat. Sci.*, *32*, 4031.
[37] Lin, Q., & Yee, A. F. (1994). *Polymer*, *35*, 2679.
[38] Amendola, E., Carfagna, C., Giamberini, M., & Pisaniello, G. (1995). *Macromol. Chem. Phys.*, *196*, 1577.
[39] Agari, Y. (1993). *J. Appl. Polym. Sci.*, *49*, 1625.
[40] Agari, Y., & Uno, T. (1985). *J. Appl. Polym. Sci.*, *30*, 2225.
[41] Giang, T., & Kim, J. (2015) *J. Ind. Eng. Chem*., 30, 77.
[42] Mormann, W., & Brocher, M. (1998). *Polymer*., *40*, 193.
[43] Mormann, W., & Brocher, M. (1998). *Macromol. Chem. Phys.*, *199*, 1935.